Evidence for the physical basis and universality of the elimination of particulates using dual-laser ablation. I. Dynamic time-resolved target melt studies, and film growth of Y_2O_3 and ZnO

Pritish Mukherjee,[a] Shudong Chen,[b] John B. Cuff, Palanikumaran Sakthivel,[c] and Sarath Witanachchi
Department of Physics, Laboratory for Advanced Materials Science and Technology (LAMSAT), University of South Florida, Tampa, Florida 33620

(Received 16 October 2000; accepted for publication 26 November 2001)

The application of a dual-laser ablation process, incorporating the addition of a synchronized CO_2 laser to the traditional excimer (KrF) laser used for the ablation of targets in thin film deposition, has been previously demonstrated to be effective in the elimination of particulates in films of Y_2O_3 [J. Vac. Sci. Technol. A **13**, 1171 (1995)]. It has been hypothesized that the efficacy of particulate removal is related to phase transformation from the solid to liquid phase prior to excimer laser ablation of the target material. In this series of two articles we present direct physical evidence of the dynamics of the phase transformation occurring on the target surface and its effect on the morphology of film growth. Pump–probe experiments have been conducted using the CO_2 laser to probe the dynamic reflectivity of the target surface on the nanosecond timescale. These experiments were conducted for a range of materials spanning a wide range of thermal conductivity including a low thermal conductivity insulator (Y_2O_3), and a sublimating oxide (ZnO), as well as a high thermal conductivity metal (Zn) to assess the universal applicability of the results. In this article (Part I) the results of these dynamic reflectivity experiments are correlated with previously reported particulate-free deposition of thin films of Y_2O_3. Similar experiments are conducted for ZnO. In both cases, the reflectivity measurements yielded times for the onset of melt at a variety of CO_2 laser fluences. Synchronization of the KrF laser to coincide with the onset of melt resulted in particulate-free film growth. The effect of mistiming on the quality of the deposited film is presented for ZnO. © *2002 American Institute of Physics.* [DOI: 10.1063/1.1435418]

I. INTRODUCTION

The problems associated with ''splashing'' or particulate deposition in the growth of thin films using laser ablation have been widely reported.[1] Such particulates create films with surface roughness and scattering sites that are undesirable for the fabrication of electronic or optical devices. The mechanisms associated with the ubiquitous deposition of droplets that range in size from the submicron to the 10 μm scale have been described in terms of the laser–target interaction as well as gas phase condensation.[2] In one regime, responsible for the larger droplets, the surface irregularities of the target such as microcracks, pits, and craters either initially existent or created during repetitive exposure to the ablating laser, are detached and ablated into the expanding plume. These have been detected in flight by a variety of techniques such as shadow photography[3] and inductively charge coupled device imaging,[4] or postdeposition by scanning electron microscopy (SEM) or scanning tunneling microscopy analysis of the deposited films. Postdeposition film analysis has also revealed the deposition of submicron droplets. These are generated as a result of the explosive ablation of a superheated subsurface molten pool splashing due to laser-induced recoil pressure in short pulse interaction,[5] or caused by supersaturated gas phase condensation or ''clustering'' at high ambient pressures.[1] The dependence of particulate formation on laser fluence, wavelength, ambient gas pressure, and other processing parameters, as well as their velocity distributions have been studied.[1,6,7]

A variety of methods has addressed aspects of the particulate problem (see, for example Ref. 8). One approach is reduction of the laser power to just above the threshold for ablation.[5] The kinetic energy of the ablated plume species is reduced in the process, thereby sacrificing the energetic advantages of laser ablation for low-substrate-temperature deposition. Mechanical filters[9,10] as well as magnetic filters[11] have been used to reduce the deposition of the larger than micron-sized particulates.[9–12] However, this results in a corresponding reduction in deposition rates and does not address the elimination of the smaller particulates effectively.[2] Rotating the target at high speeds while ablating it near the edge, causes enough deviation of the slower particulates from the original path, thereby leading to a reduction in particulate density.[2] This technique also applies to the larger particulates, as does the technique of off-axis deposition.[12] An ingenious method for the removal of larger particulates by ablation from a molten target has been demonstrated in

[a]Author to whom correspondence should be addressed; electronic mail: british@chuma.cas.usf.edu
[b]Currently at E-TEK Dynamics, 1865 Lundy Ave., San Jose, CA 95131.
[c]Currently at Axcelis Technologies Inc., 7600 Standish Place, Rockville, MD 20855.

the CO_2 laser-ablated deposition of Ge.[2] This technique is applicable primarily to those materials that have a low vapor pressure at the melting point. Also, multicomponent targets with constituents of differing volatilities will not be amenable to this approach. Postablation plume heating by a second laser has been used to vaporize the clusters ejected by the first laser.[13] This has resulted in the reduction of particulate size, but not in their removal. Reduction in both particle size and density of particulates was observed in the ablation of yttrium–barium–copper oxide (YBCO) by the Nd:Yttrium–aluminum–garnet (YAG) laser when the plume was irradiated by a second ultraviolet (UV) laser incident parallel to the target.[14] However, single UV laser ablation of YBCO yielded less particulates than this two-laser configuration.[1]

We have previously presented a dual-laser ablation technique that produced essentially particulate-free optical films of Er:doped Y_2O_3.[14] This material was used as a precursor to work on the deposition of YAG films for optical devices. The dual-laser ablation technique consists of a temporally synchronized combination of CO_2 and KrF laser pulses having wavelengths of 10.6 μm and 248 nm, with pulse widths of $\sim$200 and 20 ns, respectively.[14] These laser pulses overlap spatially on the target and are temporally adjusted to obtain particulate-free film deposition. Our experiments have demonstrated that precise control of the interpulse delay and the respective laser fluences is essential for successful particulate removal.[15]

Based on the currently understood mechanisms of particulate generation in laser ablation, the hypothesis for the success of particulate removal in dual-laser ablation is twofold. First, the CO_2 laser must arrive on the solid target prior to the KrF laser pulse in order to smoothen the surface by melting without causing any ablation. This is because the wavelength dependence of particulate deposition in laser ablation suggests that ablation by the longer wavelength CO_2 laser will, by itself, generate more particulates.[1] The KrF laser will ablate from a molten target, thereby avoiding the generation of particulates greater than 1 μm in size. The submicron particulates are subsequently evaporated in the heating of the KrF ablated plume by the remainder of the longer pulse CO_2 laser. This has been verified by spectroscopic measurements of the plasma temperature immediately following the dual-laser combination. An increase in initial plasma temperature from 7000 to 25 000 K on comparing single KrF laser to dual-laser-ablated ZnO plumes has been observed.[16] Using the line intensity ratio method,[17] time-of-flight spectroscopic measurements obtained 1 cm away from the target, for the ablation of Y_2O_3, demonstrate peak atomic temperatures for the yttrium atom in excess of 9000 K under dual-laser ablation, as compared to a corresponding temperature of 5800 K for single-laser ablation in a 20 mTorr oxygen ambient.[18]

The evidence for increased plasma temperatures under dual-laser ablation provides direct physical corroboration for the hypothesis affecting the evaporation of submicron particulates in dual-laser ablation. However, the hypothetical correlation between interpulse delay and the melting of the target for removal of the larger particulates has not been directly established. We present, in this article, direct evidence for the time of melt in both Y_2O_3 and ZnO targets, and the resultant film deposition. These two materials are chosen not only because of their practical use, but because of their similarity in thermal conductivities. Y_2O_3 has a phase-dependent thermal conductivity between 0.34 and 0.50 W/(cm K), while the corresponding value for ZnO is 0.29 W/(cm K). There is, however, a major difference in the phase transformation characteristics of these two materials. Y_2O_3 has a melting point of 2683 K and a boiling point of 4573 K, while ZnO melts and sublimes at 2248 K. Thus, even though there is a closeness in melting points, Y_2O_3, unlike ZnO, has a large range of 1890 K between the phase transformation from the molten liquid to the evaporative plume. This should lead to the formation of a deep liquid pool for molten Y_2O_3 and a shallow depth of melt for ZnO. This has consequences for particulate deposition in these two materials as it is well known that the splashing of submicron particulates is related to the formation of a superheated liquid subsurface layer.[1] Therefore, the ejection of particulates is expected to be a particularly severe problem for Y_2O_3 and less so for the sublimating ZnO. A comparison of results for the two materials will provide an assessment of the general applicability of such studies.

The remainder of the article is organized as follows. In Sec. II we describe the initial dynamic pump–probe target reflectivity setup and an improved version of the measurements incorporating a monitor for single-shot detection. A much simpler single beam method to monitor transient reflectivity is also introduced. All of these techniques are applied to Y_2O_3 targets and correlated with previous data on dual-laser-ablated film growth. Section III includes the application of the pump–probe dynamic reflectivity technique, and the single-beam method for detecting the onset of melt for ZnO, followed by results on the deposition of ZnO films using dual-laser ablation. The article ends with a discussion of the salient conclusions in Sec. IV. In a subsequent paper, (Part II), we describe the application of a modified pump–probe arrangement to detect the surface modification of a metallic target, Zn. The major distinctions between Parts I and II is that in the latter we discuss the applicability of this method of target surface studies in systems for which the signature of melt is not observable. There is also a huge difference in the regimes of thermal conductivity and optical absorption encompassed in the two articles.

II. DYNAMIC TARGET REFLECTIVITY AND FILM GROWTH OF Y_2O_3

Laser pulses rarely remove material in a clean, orderly, layer-by-layer fashion. Morphological changes can create periodic structures such as ripples, ridges, and cones.[19] When a material is exposed to a laser pulse, the absorption of pulse energy is followed sequentially by melting and vaporization. Finally, the molten material resolidifies and sometimes leaves frozen capillary waves at the surface.[19] Earlier research on studying these surface modifications and resultant theories have relied on surface images of laser-treated targets using SEMs.[19–26] But all of these focused on the surface

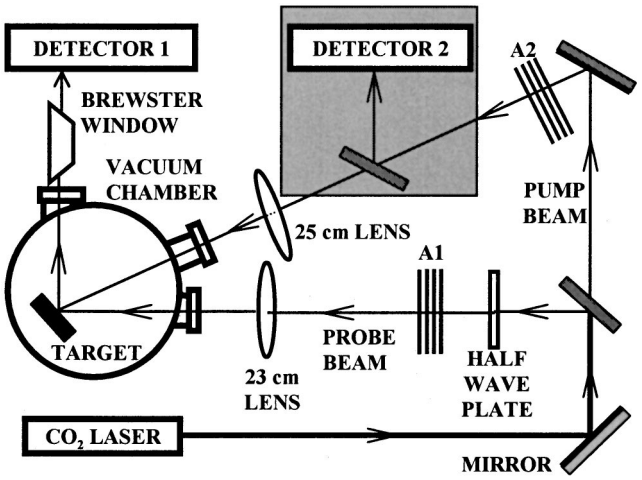

FIG. 1. The optical setup for time-resolved pump–probe surface reflectivity studies. The experimental setup for transient single-shot reflectivity included the addition of a beamsplitter and detector 2 (as shown in the gray inset).

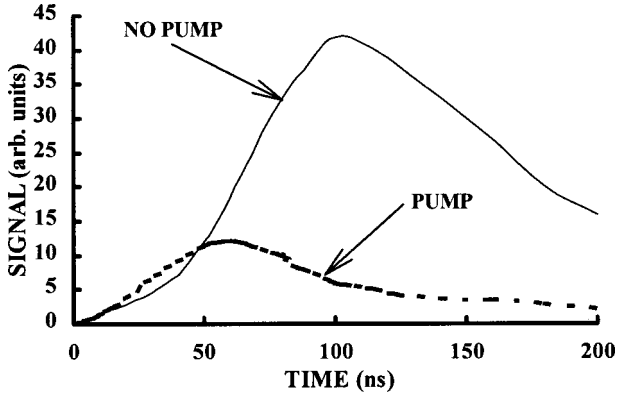

FIG. 2. Time-resolved reflected probe pulse with and without a 42.5 J/cm^2 CO_2 pump pulse incident on Y_2O_3 target.

structure after the molten material had resolidified. In our dual-laser ablation process, the dynamic modification of the target by the CO_2 laser is important and cannot be assessed by standard static postlaser treatment imaging.

Since the timing of the two lasers in the dual laser ablation system is crucially important in the growth of particulate-free films, and the KrF laser pulse is hypothesized to arrive on target precisely at the onset of melt for optimum film quality, we need to determine the transient effect of the CO_2 laser when it interacts with the target. Specifically, the melting of the target and when it occurs need to be accurately determined. Both the Y_2O_3 and the ZnO used in our study were sintered, pressed powder targets. The surfaces of the targets are therefore microscopically rough and scatter unabsorbed, incident radiation. The principle of melt detection was simply to overlap the pump and probe CO_2 beams on the target and detect the changes in the specularly reflected, time-resolved probe signal. The onset of melt is expected to smoothen the surface and cause an increase in the detected probe signal. By suitably time resolving the reflected probe, the onset of melt can be determined.

A. Pump–probe reflectivity measurements

The initial pump–probe setup is shown in Fig. 1. The output beam of a transversely excited atmospheric CO_2 laser, tuned to the 10.59 μm 10P(20) CO_2 transition, was vertically polarized using intracavity Brewster windows. A small portion of this polarized beam was split off from the main pump beam, rotated 90° using a half-wave plate, and then used as a probe of target reflectivity. Orthogonal pump–probe polarization eliminated interference effects and also allowed preferential discrimination of the probe pulse in the reflected signal by using suitably aligned Brewster windows. Rejection ratios as high as 1 in 50 were obtained. The pump beam was focused to a larger spot size on the target than the probe beam on the target to permit complete overlap. A sintered, packed powder Y_2O_3 target was used in a 20 mTorr oxygen ambient.

Temporal profiles of the probe pulse were obtained initially with only the probe beam incident onto the target. The specularly reflected probe pulses were detected by a pyroelectric detector. Subsequently, the pump beam impinged on the same spot on the target along with the probe pulse. The resultant change in the reflectivity of the target surface under laser pumping was detected by observing the time-resolved reflection of the weak probe pulse in a specular geometry. The probe pulse was kept as weak as possible so that it did not, by itself, cause any modification of the target.

Typical time-resolved probe signals, with and without a 42.5 J/cm^2 CO_2 pump pulse are shown in Fig. 2. In the presence of the pump, the specular probe signal initially increases. This enhancement at about 10 ns after the onset of pump radiation indicates the rapid formation of a molten surface. The subsequent decrease of the probe pulse signifies the ejection of a plume due to the pump pulse as it increases in intensity. This emitted plume absorbs and attenuates the latter part of the probe signal.

The extent of this initial enhancement and subsequent decrease can be represented by monitoring the relative reflectivity of the probe pulse. This is obtained as the ratio of the probe signal in the presence of the pump to that obtained in its absence. A relative reflectivity of 1 indicates no change in the target, while values greater or less than unity correspond to surface melting and plume emission (or ablation), respectively. Probe reflectivity signals were obtained at pump fluences of 5.3 and 2.1 J/cm^2, in addition to that shown in Fig. 2 at 42.5 J/cm^2. Figure 3 shows the relative reflectivities for all the pump fluences used in this study. A progressive delay in the onset of melt and decreasing absorption due to the ablated plume are observed with decreasing CO_2 fluence. For 2.1 J/cm^2, the onset of melt has moved to 60 ns after the beginning of the laser pumping and the probe signal does not drop below unity, an indication that the CO_2 pump pulse is not causing laser ablation at this fluence. This is advantageous for thin film growth as the role of the CO_2 laser should be to modify the surface by melting it, without causing any ablation.

B. Single-shot reflectivity measurements

One of the drawbacks of the previous configuration is that at least two laser shots have to be recorded in order to

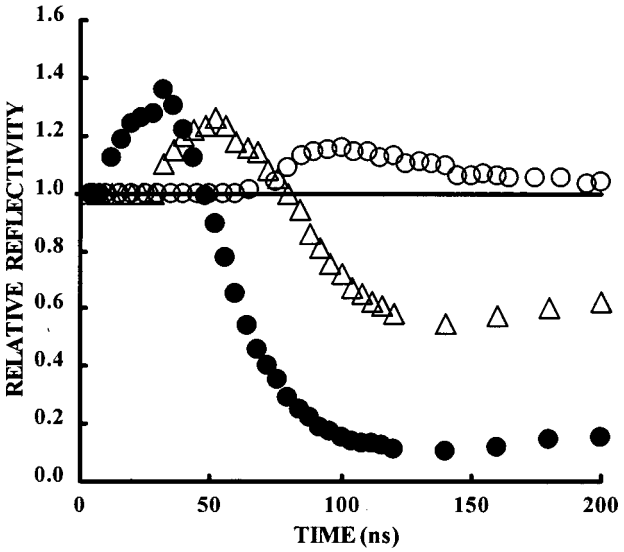

FIG. 3. Time-resolved relative reflectivity of the Y_2O_3 target at a pump CO_2 laser fluence of 42.5 J/cm^2 (solid dots), 5.3 J/cm^2 (triangles), and 2.1 J/cm^2 (open circles).

determine the onset of melt—one without the pump incident on the sample and another while the pump impinges on the target. In practice, because of the possibility of shot-to-shot energy fluctuations, data averaging over several shots would need to be used. Modification of the surface of the target can occur after each shot at the higher laser fluences for which the sample is observed to ablate. This can be overcome by rotating the target to obtain each probe reflection from a fresh spot on the target. However, that can increase the fluctuations in the specularly detected probe signal.

A simple modification to the initial optical configuration was made (see the addition of the gray inset to Fig. 1). Detector 2 was added to monitor the laser pulse shape directly, so that the scattered probe pulse could be compared to the actual laser pulse directly for each individual laser shot. Both the detectors were high sensitivity HgCdTe infrared detectors to permit single shot detection for very weak probe levels. The pump beam was focused by a 25 cm lens to an area of about 0.19 mm^2 corresponding to a laser spot size (beam radius) of $\omega = 245\ \mu$m. The probe beam was focused using a 23 cm focal length lens to confine it within the pump profile, as before. The detected probe pulses were stored using a dual-channel digital real-time oscilloscope (Tektronix Model No. TDS 380).

In the absence of the pump pulse, the detected probe pulse (detector 1) should have the same temporal profile as the monitoring pulse (detector 2). The difference in their amplitudes can be normalized. By comparison of the pulses observed by the two detectors in the absence of the pump pulse, we verified that the temporal overlap of the probe and monitor pulse shapes is almost exact. This ensured accuracy of comparison between the outputs of the two detectors when both the pump and probe pulses were turned on.

The transient single-shot probe signal obtained at CO_2 laser fluences of 6.7 and 3.1 J/cm^2 are shown in Figs. 4(a) and 4(b). Both the enhanced reflectivity signaling melt and the cutoff due to plume emission are observed.

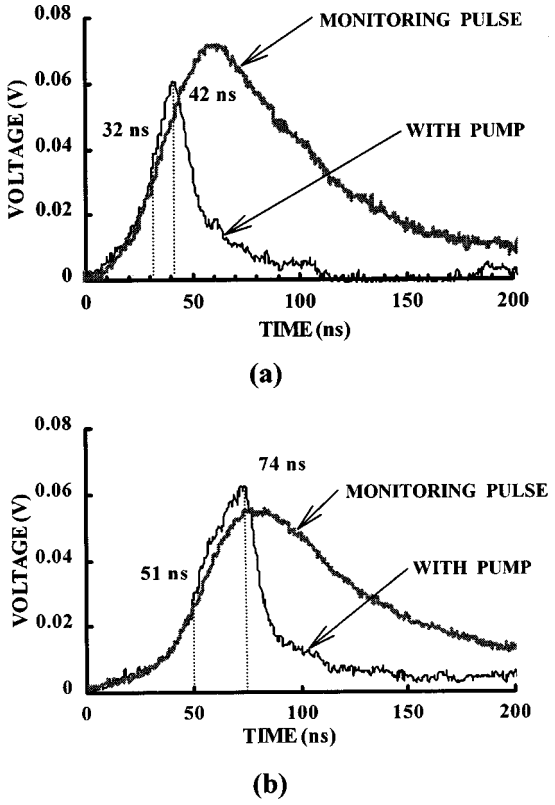

FIG. 4. Surface reflectivity of Y_2O_3 using single shot comparison. Data obtained at pump CO_2 laser fluences of: (a) 6.7 J/cm^2 and (b) 3.1 J/cm^2. The vertical lines indicate the times for the onset of melt and ablation in each case.

C. Single beam reflectivity measurements

The pump–probe configuration may be simplified to obtain information about target surface modifications by observing the temporal profile of the specularly reflected pump pulse as it interacts with the target. As the target melts, the smoothening of the surface may result in the enhancement of specular pump reflection, followed by absorptive decrease due to absorption in the self-ablated plume. This single beam configuration (Fig. 5) eliminates the probe pulse and pro-

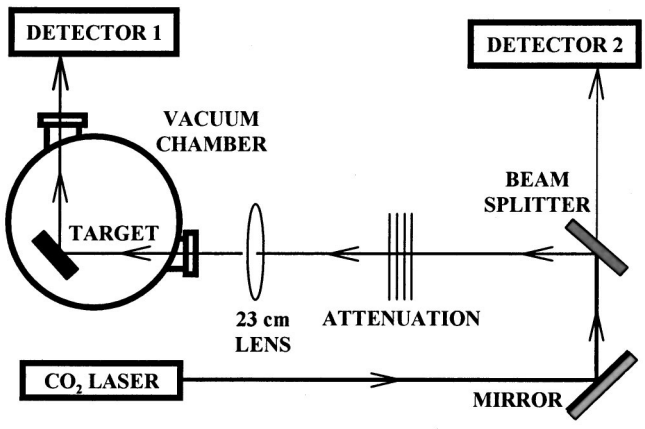

FIG. 5. The experimental setup for single beam transient reflectivity measurements.

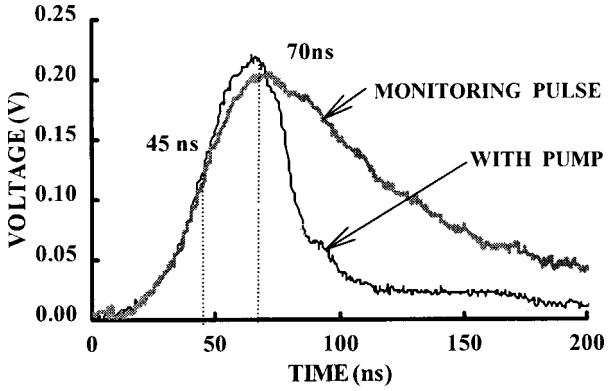

FIG. 6. Single beam data for Y_2O_3 target ablated by a 4 J/cm^2 CO_2 laser pulse. The vertical lines indicate the times for the onset of melt and ablation.

vides a simple way of monitoring the plume cutoff so that the time for melting can be calculated or, in some cases, observed directly.

One clear advantage of the single beam reflectivity method is that it makes alignment of the system very easy. This is particularly significant since our previous configurations involved ensuring the spatial overlap of invisible infrared pump and probe pulses on the target. However, a clear interpretation of the observed signal may not be straightforward in this case. For example, the onset of melt might result in enhanced coupling of the pump pulse into the target, due to multiphoton absorption processes at high pump fluences. This would result in a decrease in reflectivity and mask the true onset of melt. In the event that such a decrease is immediately evident, the onset of melt might well be signaled by a decrease in the temporal profile of the scattered pump pulse.

The data obtained on using the single beam configuration for the Y_2O_3 target at a CO_2 laser fluence of 4 J/cm^2 is shown in Fig. 6. In this case, both melting and cutoff due to the plume were still detectable by this system. The time of ablation and melting are observed to be 70 and 45 ns, respectively.

D. Film growth

In our deposition experiments, the KrF laser fluence was adjusted to 1.2 J/cm^2 for both Y_2O_3 and the subsequently described ZnO films (in Sec. III C), which ensured that it was above the ablation threshold in each case. The KrF laser spot size on the target was 9 mm^2 and spatially overlapped the CO_2 laser spot for the dual-laser ablated deposition. A 45° angle of incidence was used for the lasers on the target. However, this is not crucial, as the plume is always emitted perpendicular to the target, irrespective of the angles of incidence of the ablating lasers. The films were deposited on room temperature Si substrates.

The time to ablate, as well as the time to melt the Y_2O_3 target as a function of incident CO_2 laser fluence, can be determined based on the data obtained using the three different techniques. The results are shown in Figs. 7(a) and 7(b), which includes all the data acquired using the three different methods discussed above. The plots show a decreasing trend

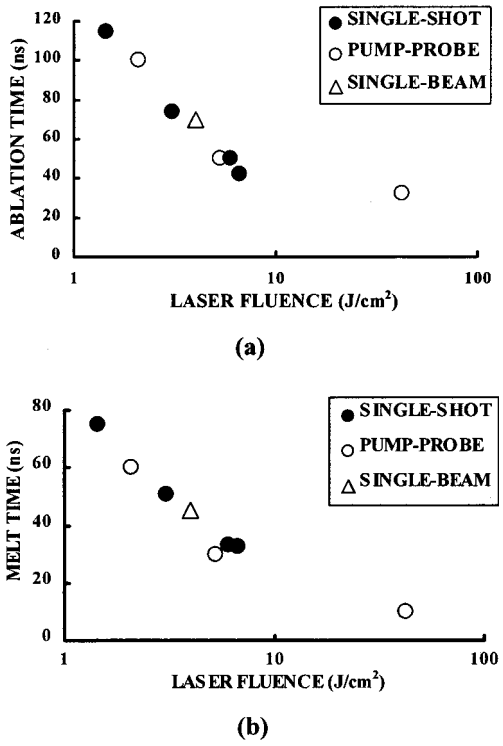

FIG. 7. (a) Time of ablation and (b) time of melt vs varying CO_2 laser fluences for Y_2O_3.

for both ablation time and melt time as the laser fluence increases. The data acquired with different techniques are consistent with each other, which shows that these techniques are reliable in studying target–surface phase transformations. The conformity of the single beam result within the general trend indicates that, at least for poor conductors at reasonable CO_2 laser fluences even when some ablation is evident, this technique is useful.

A reasonably long melt duration is desirable in dual-laser thin film deposition for ease of synchronization between the KrF and CO_2 lasers. A second consideration is lack of ablation by the CO_2 laser itself. This is clearly the case for the 2.1 J/cm^2 relative reflectivity data in Fig. 3. However, somewhat higher CO_2 fluences for which there is ablation of Y_2O_3 late in the CO_2 laser pulse would also be suitable for particulate-free film growth, while allowing more of the CO_2 laser pulse energy to be absorbed in the KrF laser generated plasma. This will lead to higher plasma temperatures that will evaporate any remaining submicron particulates and provide higher plume energies for low substrate temperature deposition. The ideal situation is therefore one in which the highest CO_2 laser fluence is used such that the ensuing KrF laser ablated plume is able to absorb all of the remaining CO_2 laser energy without causing any further ablation.

Our data in Fig. 7 are consistent with the previously reported optimum conditions of 50 ns interpulse delay at a CO_2 laser fluence of 3.5 J/cm^2 for a significant reduction of particulate density on the deposited Y_2O_3 films.[14] Films have been deposited at a CO_2 laser fluence of 3.5 J/cm^2 for a 50 ns interpulse delay as well as a delay of 150 ns at which the peaks of the KrF and the CO_2 laser pulses coincide. The

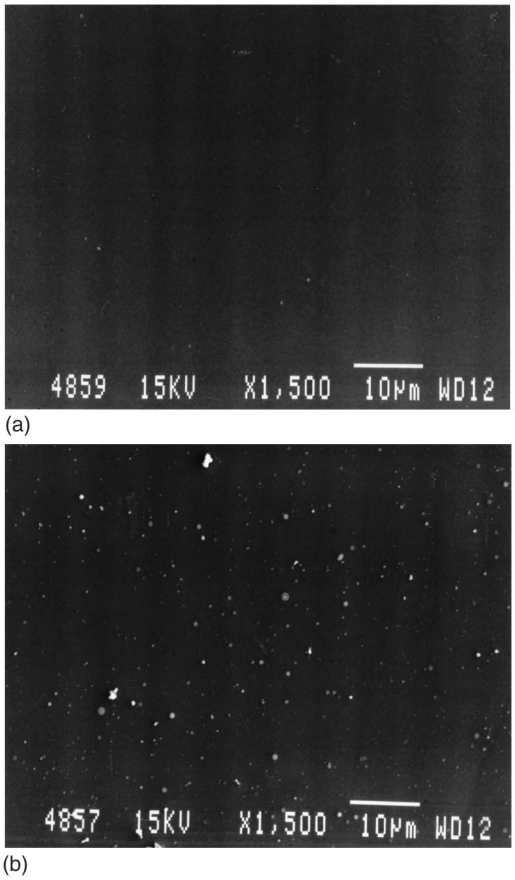

FIG. 8. SEM of Y_2O_3 under dual laser ablation at a KrF laser pulse delay of: (a) 50 ns and (b) 150 ns after the onset of the CO_2 laser pulse.

corresponding SEMs are shown in Figs. 8(a) and 8(b), respectively. The Y_2O_3 film deposited at a delay of 50 ns, coincident with the onset of melt in Fig. 7(b), is virtually particulate-free [Fig. 8(a)]. Changing the interpulse delay to 150 ns goes beyond the 90 ns time for ablation by the CO_2 laser at 3.5 J/cm^2, thereby leading to the deposition of particulates in the deposited film [Fig. 8(b)]. This confirms the hypothesis that the role of the CO_2 laser pulse in the deposition of particulate-free Y_2O_3 films is directly related to melting the target prior to KrF laser ablation.

III. DYNAMIC TARGET REFLECTIVITY AND FILM GROWTH OF ZnO

We will focus, in this section, on the transient reflectivity measurements on the ZnO target and the deposition of particulates in the resultant films. The ZnO used was a commercial, sintered, packed powder target that was insulating. It was a yellowish ceramic, with a melting point of 2248 K, and it sublimes at the same temperature. Two different techniques were used in determining the transient melt characteristics. They are the single shot comparison using a monitor and the single beam configurations described earlier in Secs. II B and II C, respectively.

A. Single-shot reflectivity measurements

With the method of single shot comparison, the ZnO target was tested at different CO_2 pump laser fluences of 2.67, 5.74, 8.41, and 12.86 J/cm^2. Both the melting process and cutoff due to the plume were repetitively observed. Representative data at these various CO_2 laser fluences, with melt and ablation times labeled, are shown in Figs. 9(a)–9(d).

Over the range of laser fluences studied, the time of melt changes from ~40 to ~30 ns after the onset of the CO_2 laser pulse. A plot of the time of ablation at different laser fluences is shown in Fig. 10(a) (circles). Similar to Y_2O_3, at higher laser fluences, the emission of the plume is obviously earlier than that at a lower fluence. The energy needed to ablate the ZnO target for the different laser fluences was also calculated by integrating the corresponding area under the pump pulse. The results are shown by the circles in Fig. 10(b). For ZnO the energy needed for melt/ablation is approximately constant, independent of the pump pulse fluence.

B. Single beam reflectivity measurements

The ZnO target was also investigated using the single beam configuration. Results similar to those for the single-shot pump–probe experiments reported in the previous subsection were obtained. Representative data are shown in Fig. 11. The results for the initial ablation time versus laser fluence are shown by the triangles in Fig. 10(a). The triangles in Fig. 10(b) demonstrate that the energy needed for melting ZnO at different laser fluences is constant. A comparison of all the data presented in Figs. 10(a) and 10(b) demonstrates remarkable consistency in the determination of ablation times as well as the energy needed to ablate the target at each CO_2 laser fluence. Therefore, both the techniques used show a constant requirement of laser energy to cause the material to ablate [Fig. 10(b)]. For ZnO, independent of the rate at which the pump laser energy is incident on the target, there is insufficient dispersion of the energy in the material during the laser pulse due to the low thermal conductivity of the target. Consequently, it needs approximately constant energy to vaporize the material, independent of incident laser fluence. Another interesting feature of the single shot transient reflectivity data is the presence of oscillations in the reflectivity at the highest laser fluence of 15.3 J/cm^2. This is related to the sublimation of ZnO and is discussed later.

Our study of the ZnO target with the single beam configuration and its agreement with results obtained using the pump–probe configuration, showed the possibility of studying surface phase transformations using a single laser beam only. This configuration has the same reliability as the conventional pump–probe configuration without the complicated optical alignment necessary for pump–probe experiments, and is thus a useful technique for use in future studies.

C. Film growth

ZnO crystallizes in the hexagonal wurtzite structure and has a large band gap of 3.2–3.3 eV.[27,28] It has applications as a photoconducting, semiconducting, optical waveguiding, and piezoelectric material. The electrical conductivity of ZnO is controlled by interstitial Zn atoms, and by Zn and O vacancies. The deposition of conductive ZnO films by ablat-

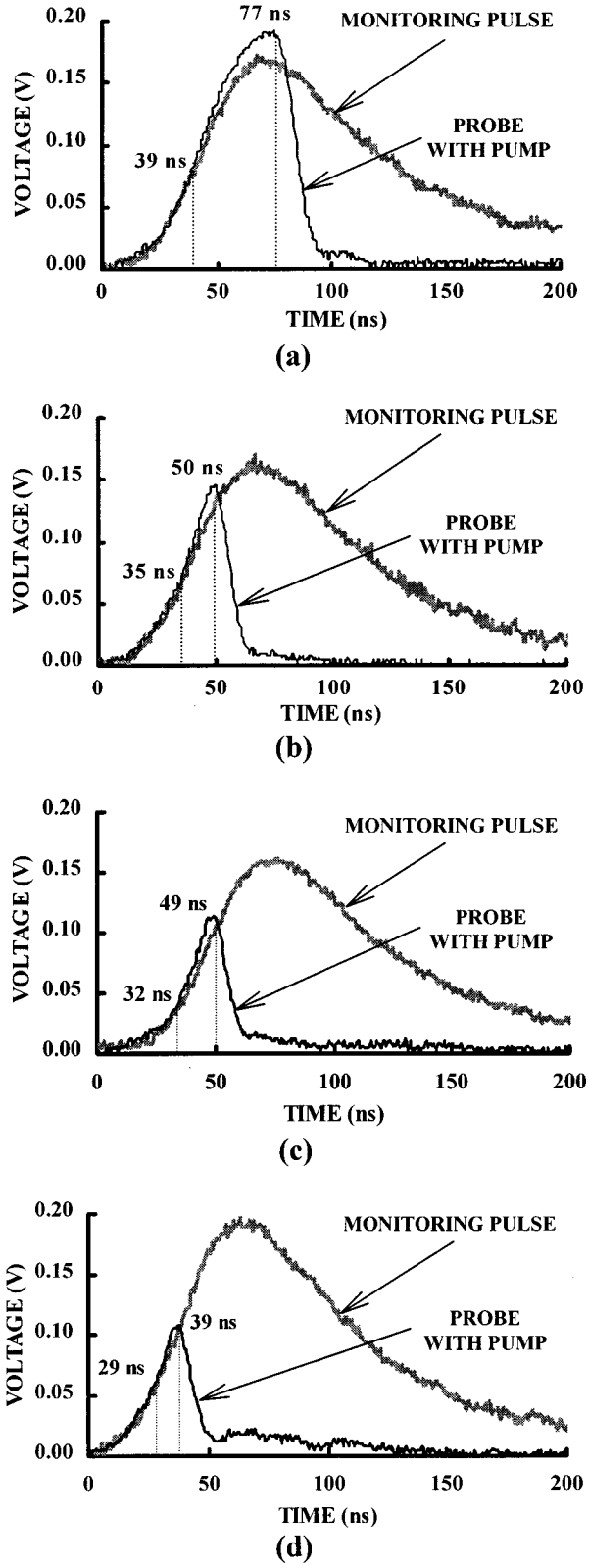

FIG. 9. Surface reflectivity of ZnO using single shot comparison, at pump CO_2 laser fluences of: (a) 2.67 J/cm^2, (b) 5.74 J/cm^2, (c) 8.41 J/cm^2, and (d) 12.86 J/cm^2. The vertical lines indicate the times for the onset of melt and ablation in each case.

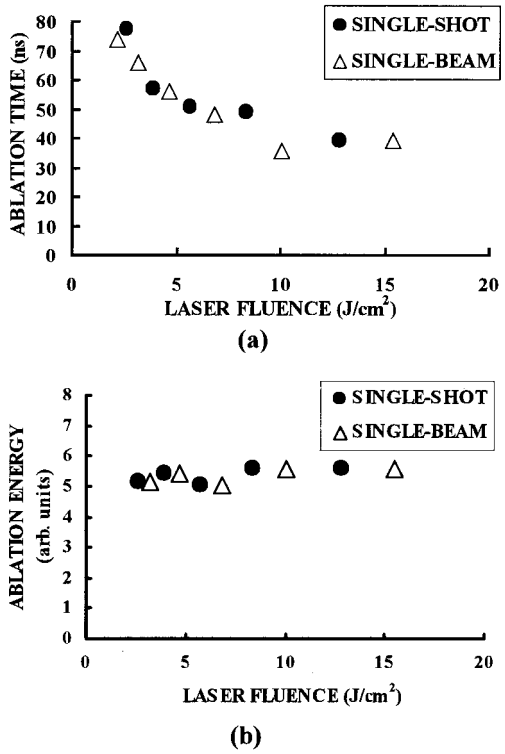

FIG. 10. A plot of (a) the time of ablation and (b) the energy needed for ablation of ZnO at different CO_2 laser fluences using two different techniques.

ing ZnO in an oxygen ambient has been reported.[29] Electrical resistivities range from $10^2-10^4\ \Omega$ cm in one study[30] to $10^{-2}-10^{-4}\ \Omega$ cm in another.[27] Doping by fluorine, aluminum, gallium, and indium can help overcome the low dc conductivity of ZnO and exploit its semiconducting characteristics. Doped samples with resistivities below $3\times10^{-4}\ \Omega$ cm have been reported.[31] The O vacancies play an important role in conductivity and result in *n*-type doping in films with carrier concentrations on the order of $10^{19}-10^{20}$ cm^{-3}.[27,28,31] We have ablated Zn in an oxygen ambient at various partial pressures and obtained highly conductive ZnO films with a maximum conductivity of 10^3 $(\Omega\,\mathrm{cm})^{-1}$ at an ambient pressure of 20 mTorr of oxygen for dual-laser ablation.[29] For the experiments reported in this article, the ZnO target was ablated using dual-laser ablation and deposition in 10 mTorr of ambient oxygen under dual-laser ablation resulted in highly conductive ZnO films.

In order to minimize the temporal fluctuations between the two lasers, we used an optical triggering scheme for the interpulse synchronization.[32] As opposed to standard electronic triggering techniques, we used the optical flash from the high voltage discharge of the CO_2 laser to trigger the KrF laser. This resulted in improved shot-to-shot reproducibility and an accuracy in the temporal positioning of the KrF laser with respect to the CO_2 laser that was better than 10 ns.[32]

Films of ZnO were deposited using the optical triggering technique at a CO_2 laser fluence of 5.6 J/cm^2. The onset of melt at this fluence can be estimated to be at 35 ns based on the transient reflectivity data [see Fig. 9(b)]. An SEM of the film made with the KrF laser pulse at this onset of CO_2 laser induced melt is shown in Fig. 12(a). The film is essentially particulate free. On moving the timing of the KrF laser pulse 40 ns prior to the onset of the CO_2 laser on the ZnO target the film shows evidence of significant particulate deposition

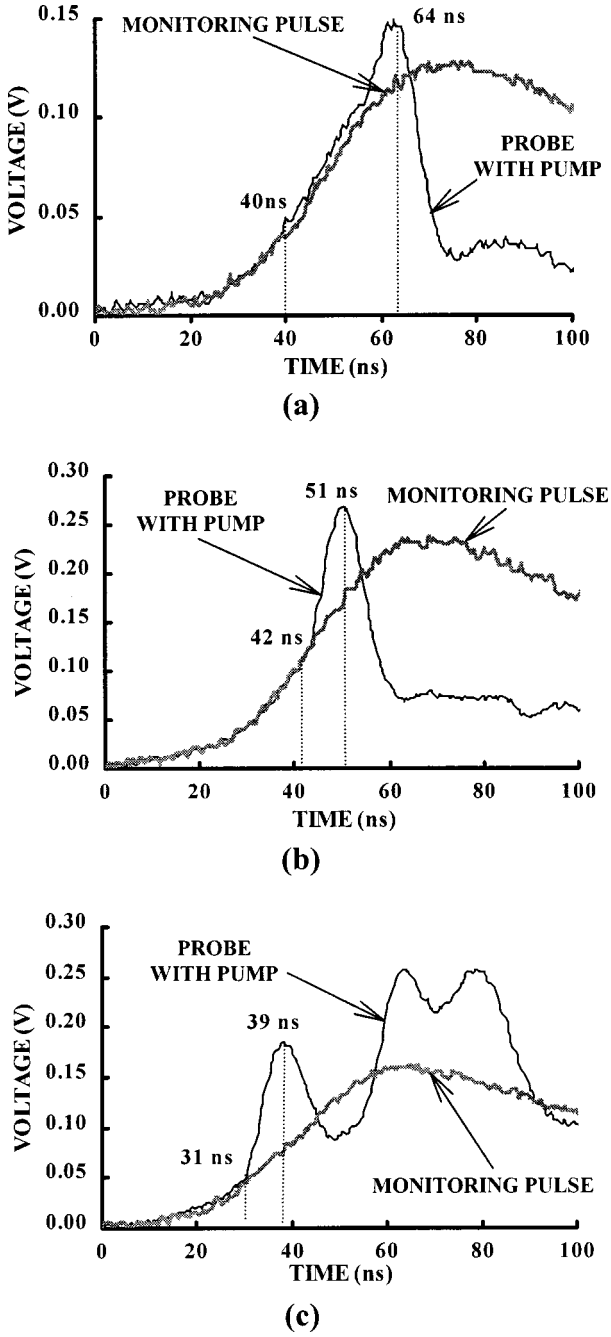

FIG. 11. ZnO reflectivity data with single beam configuration, at a CO_2 laser fluence of: (a) 3.2 J/cm^2, (b) 10 J/cm^2, and (c) 15.3 J/cm^2. The vertical lines indicate the times for the onset of melt and ablation in each case.

[Fig. 12(b)]. The CO_2 laser pulse is able to evaporate the micron-sized particulates that are ablated by the KrF laser impinging on a solid ZnO target in this case. However, a distribution of particulates, ranging from ~10 nm to some greater than ~150 nm, is evident in Fig. 12(b). This provides direct evidence that ablation of the ZnO target, lacking the onset of melt, perpetuates the splashing problem.

The substantial lack of particulates at a CO_2 laser fluence of 5.6 J/cm^2 [in Fig. 12(a)], even though it would cause ablation in the absence of the KrF laser, indicates that the KrF laser-ablated plume is an efficient absorber of the CO_2 laser pulse remaining after the first 35 ns. This screens the

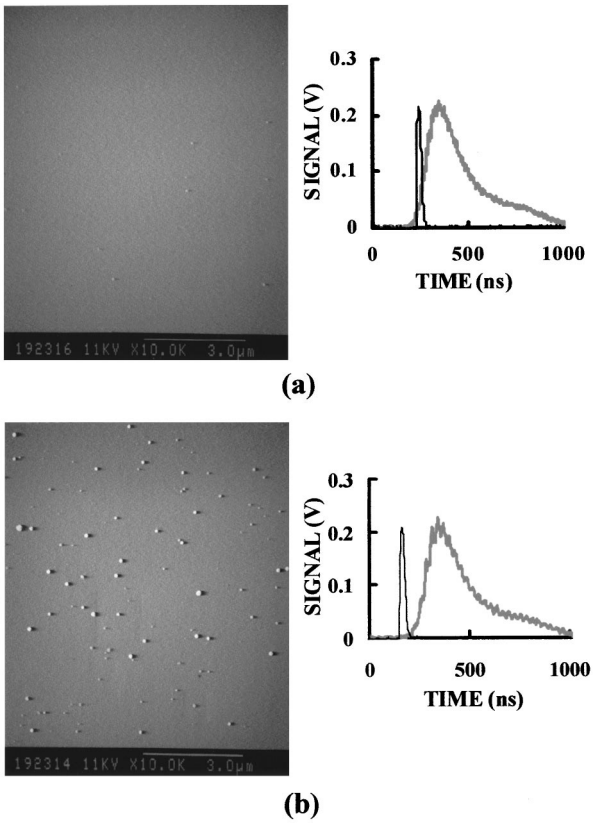

FIG. 12. SEMs of ZnO films deposited using dual laser ablation, with the KrF laser: (a) 35 ns after and (b) 40 ns before the onset of the CO_2 laser pulse.

target from the remainder of the CO_2 laser pulse, thereby making it effective in the evaporation of any ejected submicron particulates, without causing any ablation by the CO_2 laser itself.

IV. DISCUSSION AND CONCLUSIONS

The data on the reflectivity of ZnO clearly shows that even though ZnO sublimes at its melting point, its molten state still exists for a finite duration. The observed finite melt duration is a consequence of the Gaussian spatial intensity profile of the pump CO_2 laser. The center gains more energy first, and melts first. Areas adjacent to the center acquire energy to melt starting outward from the center. As the melt propagates outward, the area of the molten surface increases in time, thereby causing a dynamic increase in the probe reflectivity. Significant ablation occurs subsequent to the melting of a spot equal to the size of the focused beam spot on the target. The time that it takes to propagate this distance can be obtained from the surface reflectivity data (Figs. 7 and 11); it is the time interval between when the reflectivity starts to increase and when it starts to decrease. From the propagation distance and time, the velocity of propagation of the surface melt can be found. A plot of this velocity versus laser fluence is shown in Fig. 13. As physically expected, the melt propagation velocity increases almost linearly with laser fluence due to the increased spatial gradient of laser intensity at higher fluences.

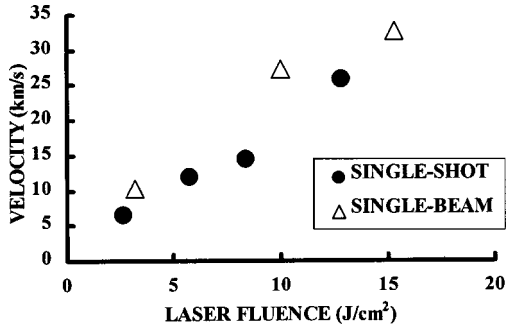

FIG. 13. Lateral melt propagation velocity for ZnO determined by two different techniques.

Another interesting observation is the presence of three oscillations in the transient reflectivity of the scattered pump pulse under high CO_2 fluence irradiation [Fig. 11(c)]. This is not observed for Y_2O_3. The oscillations provide direct evidence of the sublimation of ZnO. At the high CO_2 fluence, the ablation takes place by the removal of several successive layers during the laser pulse. Each cycle of the oscillation corresponds to energy absorption, melting, and simultaneous evaporation starting from the center of the irradiated spot and then spreading out (leading to the observed decrease in the reflectivity due to absorption of the pump pulse in the ablated plume). The increased reflectivity that follows indicates the onset of melt for the next layer and so on. This characteristic is a general phenomena for sublimating targets. Obviously, these cycles are not observable using either of the pump–probe techniques because the probe is completely attenuated subsequent to the ablation from the first cycle.

In conclusion, the transient target surface phase transformations under CO_2 laser irradiation, including both melting and vaporization, have been observed and recorded for Y_2O_3 and ZnO by three different methods. Repeating the measurements with various techniques developed confidence in our techniques as well as in the reliability of the determinations of the onset of melt and ablation in the two materials. Despite the differences in phase transformation, the agreement of the observed onset of melt with the timing for particulate-free film growth for both target materials provided direct evidence for the physical mechanism operative in particulate removal under dual-laser ablation. These results on low thermal conductivity materials will be extended in Part II to a highly conductive metallic target to establish the universal applicability of this method.

ACKNOWLEDGMENT

This research was supported in part by the National Science Foundation through Grant Nos. DMI-9622114, DMI-9978738, and DMI-0078917.

[1] L-C. Chen, *Pulsed Laser Deposition of Thin Films* (Wiley, New York, 1994), pp. 167–198.
[2] J. T. Cheung and H. Sankar, CRC Crit. Rev. Solid State Mater. Sci. **15**, 63 (1988).
[3] A. Gupta, B. Braren, K. G. Casey, B. W. Hussey, and R. Kelly, Appl. Phys. Lett. **59**, 1302 (1991).
[4] D. Geohegan, Mater. Res. Soc. Symp. Proc. **285**, 27 (1993).
[5] J. T. Cheung, Appl. Phys. Lett. **43**, 255 (1983).
[6] A. Matsunawa, S. Katayama, A. Suzuki, and T. Ariyasu, Trans. Jpn. Weld. Soc. Res. Inc. **15**, 61 (1986).
[7] G. Koren, A. Gupta, R. J. Baseman, M. I. Lutwyche, and R. B. Laibowitz, Appl. Phys. Lett. **55**, 2450 (1989).
[8] D. H. Lowndes, in *Laser Ablation and Desorption*, edited by J. C. Miller and R. F. Haglund, Experimental Methods in the Physics of Sciences (Academic, New York, 1998), p. 475.
[9] W. P. Barr, J. Phys. E **2**, 2 (1969).
[10] D. Lubben, S. A. Barnett, K. Suzuki, S. Gorbatkin, and J. E. Greene, J. Vac. Sci. Technol. B **3**, 968 (1985).
[11] R. Jordan, D. Cole, and J. G. Lunney, Appl. Surf. Sci. **109/110**, 403 (1997).
[12] R. J. Kennedy, Thin Solid Films **214**, 223 (1992).
[13] G. Koren, R. J. Baseman, A. Gupta, M. I. Lutwyche, and R. B. Laibowitz, Appl. Phys. Lett. **56**, 2144 (1990).
[14] S. Witanachchi, K. Ahmed, P. Sakthivel, and P. Mukherjee, Appl. Phys. Lett. **66**, 1469 (1995).
[15] S. Witanachchi and P. Mukherjee, J. Vac. Sci. Technol. A **13**, 1171 (1995).
[16] P. Mukherjee, S. Chen, and S. Witanachchi, Appl. Phys. Lett. **74**, 1546 (1999).
[17] M. W. Blades, in *Inductively Coupled Plasma Emission Spectroscopy*, Part 2 (Wiley, New York, 1987), pp. 395–399.
[18] P. Sakthivel, Ph.D. dissertation, University of South Florida, 1995.
[19] S. R. Foltyn, in *Pulsed Laser Deposition of Thin Films* (Wiley, New York, 1994).
[20] D. B. Geohegan *et al.*, J. Mater. Res. **3**, 1169 (1988).
[21] A. Hoffman, Supercond. Sci. Technol. **3**, 118 (1990).
[22] S. R. Foltyn *et al.*, Mater. Res. Soc. Symp. Proc. **191**, 205 (1990).
[23] S. R. Foltyn, R. C. Dye, K. C. Ott, E. Peterson, K. M. Hubbard, W. Hutchinson, R. E. Muenchausen, R. C. Estler, and X. D. Wu, Appl. Phys. Lett. **59**, 594 (1990).
[24] G. L. Doll, T. A. Perry, and J. A. Sell, Mater. Res. Soc. Symp. Proc. **201**, 207 (1991).
[25] J. F. Young, J. E. Sipe, and H. M. van Driel, Phys. Rev. B **30**, 2001 (1984).
[26] D. J. Krajnovich and J. E. Vasquez, J. Appl. Phys. **73**, 3001 (1992).
[27] V. Craciun, J. Elders, J. G. E. Gardeniers, and I. W. Boyd, Appl. Phys. Lett. **65**, 2963 (1994).
[28] R. D. Vispute *et al.*, Appl. Phys. Lett. **70**, 102 (1997).
[29] S. Witanachchi, Y. Ying, A. M. Miyawa, and P. Mukherjee, Mater. Res. Soc. Symp. Proc. **483**, 185 (1998).
[30] S. Hayamizu, H. Tabata, H. Tanaka, and T. Kawai, J. Appl. Phys. **80**, 787 (1996).
[31] A. Suzuki, T. Matsushita, N. Wada, Y. Sakamoto, and M. Okuda, Jpn. J. Appl. Phys., Part 2 **35**, L56 (1996).
[32] P. Mukherjee, J. B. Cuff, and S. Witanachchi, Rev. Sci. Instrum. **72**, 2380 (2001).